Journal of Hydrology X 20 (2023) 100158

Contents lists available at ScienceDirect

Journal of Hydrology X

journal homepage: www.sciencedirect.com/journal/journal-of-hydrology-x

Research papers

Water–soil interactions: Unravelling the processes and stages involved in the wetting of water repellent soils

Helen M. Balshaw [a,1,*], Peter Douglas [b,c,2], Stefan H. Doerr [d]

[a] College of Engineering, Swansea University, Bay Campus, Fabian Way, Crymlyn Burrows, Swansea SA1 8EN, UK
[b] Chemistry Group, College of Medicine, Swansea University, Singleton Park, Swansea SA2 8PP, UK
[c] School of Chemistry and Physics, University of KwaZulu-Natal, Durban, South Africa
[d] Department of Geography, Swansea University, Singleton Park, Swansea SA2 8PP, UK

ARTICLE INFO

Keywords:
Soil physics
Soil hydrophobicity
Kinetics
Contact angle
Infiltration

ABSTRACT

The water repellent behaviour of soils is a widely studied phenomenon given its implications for infiltration, runoff, erosion and preferential flow. However, the principles underlying the eventual penetration of water into affected soils remain poorly understood. Theoretical considerations of the energetics and kinetics involved as a water drop makes contact with a water repellent soil surface and eventually penetrates into the soil suggest three distinct stages in the overall process. These stages are 1) adhesional wetting as soil and water first make contact, followed by 2) a kinetic barrier transitional stage in which molecular reorganisation of organics on soil reduces the water-soil contact angle to allow the water drop to sit deeper over soil particles of initial contact such that there is contact with particles in directly underlying soil layers, and finally 3) branching interstitial wetting as water penetrates into the bulk soil. Studies presented here of optical microscopy, mass of soil initially wetted, penetration time through layers of soil of different thicknesses, and time-dependent measurements of contact angle, volume of water penetrated, and mass of soil wetted, all give results consistent with this model. However, only for highly water repellent soils can distinct stages in wetting be clearly resolved experimentally, presumably because only these soils have a high enough kinetic barrier in the transitional stage for good separation between stages. For less water repellent soils, while the general time dependent behaviour remains consistent with the model, the distinction between the three stages is not so easy to resolve experimentally. The roles of contact angle, particle size distribution and drop size in determining the rates of these stages is considered, and the implications of the model for understanding soil water repellency are discussed.

1. Introduction

Soil water repellency is the reduced ability of affected soils to absorb water and become wetted. It is thought to be caused by organic compounds with hydrophobic (non-polar) properties present as coatings on soil grains (Roberts and Carbon, 1972; Bisdom et al., 1993; Doerr et al., 2000) and in interstitial matter (Franco et al., 2000). These compounds can be derived from leaf surface waxes (McIntosh and Horne 1994), fungal and microbial activity (Jex et al., 1985; Hallett et al., 2001), plant roots (Dekker and Ritsema 1996; Doerr et al., 1998) and lipids from decomposing litter (McGhie and Posner, 1981) and lead to enhanced water repellency. It can have substantial environmental consequences such as increased overland flow leading to soil erosion, mass movement and flooding, especially after wildfires, as well as poor uptake of agricultural chemicals (Doerr et al., 2000). The latter increases the risk of crop disease, reduces yields and thus threatens food security and production (Bond, 1972). Soil water repellency also increases the risk of groundwater pollution by accelerating transfer of contaminants and nutrient leaching (Bisdom et al., 1993; Ritsema and Dekker, 1996; Hallett et al., 2001) via uneven wetting and preferential flow pathways (Dekker and Ritsema, 1994; Dekker et al., 2000).

Two experimental methods for the assessment of soil water repellency commonly used are: the water-soil contact angle, which is used to provide a measure of the initial water repellency; and the Water Drop

* Corresponding author.
E-mail address: hbalshaw@hotmail.co.uk (H.M. Balshaw).
[1] Present address: 1 Rosewarne Close, Llantilio Pertholey, Abergavenny, NP7 6QA, UK.
[2] Present address: The Conceptual Shed, 23 Meadow View, Dunvant, Swansea, SA2 7UZ, UK.

https://doi.org/10.1016/j.hydroa.2023.100158
Received 30 May 2023; Received in revised form 28 July 2023; Accepted 9 August 2023
Available online 20 August 2023

Penetration Time Test (WDPT) which measures the time for a water drop to fully penetrate the soil (Letey, 1969; Doerr, 1998; Letey et al., 2000). When measuring soil WDPT for previous studies (Balshaw et al., 2021) we often observed, particularly with highly water repellent soils, that the process of water penetration appears to be a multistage process, whereby initial contact of the water drop with the soil quickly initiates the lifting of soil grains up and around the water drop, but this is then followed by an induction period where little happens and the water drop sits on the soil until at some critical time there is more rapid infiltration of the soil as if some kinetic barrier to infiltration has been overcome. We have been intrigued by this behaviour over the years and curious to see if this multistage behaviour could be quantified and understood from both theoretical and experimental viewpoints in order to provide a conceptual model of what is involved when a water drop penetrates soil.

In general, we can envisage at least three stages in soil wetting. The initial process is the rapid initial water/soil contact, i.e. adhesional wetting; the final process is branching interstitial wetting as water penetrates the interstices of bulk soil; and whether or not an additional intermediate stage, to transition between adhesional wetting and branching interstitial wetting, is required depends on the initial degree of soil water repellency, i.e. the water-soil contact angle. Shirtcliffe et al. (2006) have calculated a critical contact angle of 50° below which adhesional wetting may lead immediately to interstitial wetting. While such low contact angles may occur in soils of very low repellency, for soils of moderate to high water repellency, i.e. those which have contact angles higher than this critical contact angle, there must also be an intermediate process which allows the transition between these two wetting regimes. The degree to which these three stages can be distinguished experimentally will depend, to a large extent, on the soil water repellency.

In an attempt to understand these processes, and to determine if the stages could be distinguished experimentally, we studied a number of sandy soils of differing water repellency using a number of relatively simple techniques, described in detail in the following section, which allow the complete process of wetting, from initial adhesional wetting through to the end of branching interstitial wetting, to be followed. Goniometer time-lapse imaging, and optical microscopy, were used to follow wetting by single drops in real time. A 'start-stop' method of collecting the mass of soil wetted at a given time after the drop was applied to the soil was used by combining data from different drops at different stop times to give pseudo time-lapse data with each data point obtained using a different water drop. A similar approach was used in a study of the size and dimensions of the wetted water pellet as a function of time, with the solid pellet obtained by freezing with liquid nitrogen. Experiments were also carried out on water drop penetration times through soil layers of increasing thicknesses to build up data on the rate of movement of the drop through the soil at various spatial stages in wetting.

2. Materials and methods

2.1. Materials

Studies were primarily focused on four naturally water-repellent sandy soils of the type we have used in previous work. Of these, three were from Gower, South Wales: two dune soils from Nicholaston, NIC1 and NIC2, and a dune soil under pine forest from Llanmadoc, LLAN1, and the other from the Netherlands, NL1, (Balshaw, 2019; Doerr et al., 2005). In addition to these soils, a study of the size of wetted soil pellets as a function of time was made using a sandy soil from Australia, AUC (wettable), which we have used in previous studies (Doerr et al., 2005) and which was chosen because it had a suitable WDPT for that particular experiment; and the profilometry data shown in Fig. 5 was obtained using a dune soil from Nicholaston, Gower, UKC (wettable), which had previously been used by our group (Doerr et al. 2005). Soil samples were taken from 0 to 10 cm depth. After collection, soils were oven dried at

Table 1
Source locations and soil characterisation of the soils used.

Code	Country	Site location, Region	Lat/Long	Vegetation type	Sample depth (cm)	Mean diameter (mm)	Total carbon content (g kg^{-1})	Water repellency class*	Bulk density loose-packed (g cm^{-3})	Bulk density settle-packed (g cm^{-3})	Mean particle diameter (μm)	Fractional void space	Average total carbon (Wt %)
UKC	Wales	Nicholaston, Gower	51°35'N 04°06'W	N/A – bare dune	0.10	0.39	[a]2.5 ± 0.5	Wettable	–	–	435.3 ± 3.5	–	–
AUC	Australia	Pine Views, Naracoorte	36°30'S 140°42'E	Cropland	0–10	0.24	[b]2.2 ± 0.4	Wettable	–	–	–	–	–
NIC2	Wales	Nicholaston, Gower	51°34'N 4°7'W	Dune grass	0–10	0.33	[c]6.7 ± 0.7	Strongly	1.443	1.598	334.9 ± 1.8	0.397	0.67 ± 0.07
LLAN1	Wales	Llanmadoc, Gower	51°37'N 4°15'W	Pine forest	0–10	0.27	[d]21.9 ± 4.4	Strongly	1.208	1.459	274.0 ± 0.3	0.450	2.19 ± 0.44
NIC1	Wales	Nicholaston, Gower	51°34'N 4°7'W	Dune grass	0–10	0.32	[c]4.5 ± 0.3	Severely	1.418	1.603	322.7 ± 0.5	0.395	0.45 ± 0.03
NL1	Netherlands	Zuid Holland, Ouddorp	51°48'N 03°54'W	Grass/moss	0.10	0.27	[a]5.1 ± 1.1	Severely-extremely	1.184	1.405	286.9 ± 4.4	0.470	1.52 ± 0.33

[a] Previous work using soils obtained from a similar Nicholaston location recorded 27% inorganic carbon as part of the total carbon present (Personal communication, Hallin, 2019). In this work the shape of the peak detection curves for total carbon analysis indicates an inorganic carbon contribution of ≤~20%.
[b] Previous work by Doerr et al. (2005).
[c] In this work an assessment of the detection curves for Llanmadoc soils indicates a contribution of ≤ ~20%.
[d] In this work an assessment of the detection curves for Llanmadoc soils indicates a contribution of ≤ ~10 %.
* Determined from WDPT test and classification of Bisdom et al. (1993).

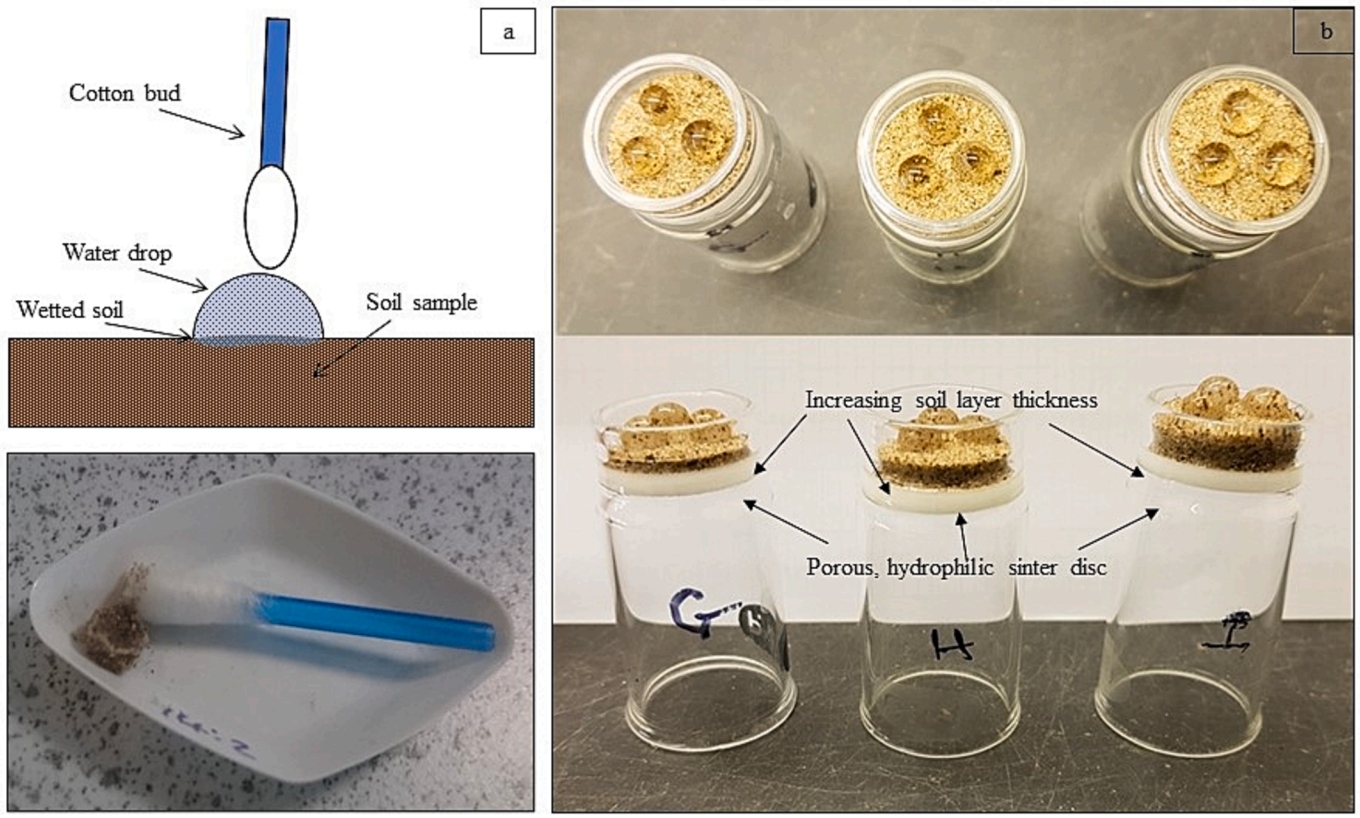

Fig. 1. Experimental set-up for (a) mass removal and (b) sinter based water drop penetration time studies. (a) Schematic of cotton bud being brought into contact with a water drop (top) and example of mass removed sample using the cotton bud method (bottom). (b) Image showing soils of varying thickness on top of a glass sinter disc.

30 °C for 48 h and then sieved using a 2-mm sieve to remove any large pieces of organic debris. Details of the soils used are given in Table 1. Distilled water was used throughout.

2.2. Methods

2.2.1. Particle size

Particle size distributions and mean particle diameter were measured using a Beckman Coulter LS Series Laser Diffraction Particle Size Analyser; the data presented in Table 1 is the average of triplicate runs.

2.2.2. Total carbon content

Total carbon content of samples was measured using a SKALAR Primacs Solid Sample TOC Analyzer. Bulk samples were ground to $<$ 250 μm using a mortar and pestle and three replicates, each weighing approximately 1000 mg, were measured for total carbon by combustion at 1050 °C. Previous work with NL and UKC soils has shown the inorganic carbon content to be negligible and total carbon content to be organic in origin (Doerr et al., 2005). Previous work using soils obtained from a similar Nicholaston location to that of NIC1 and NIC2 soils recorded 27% inorganic carbon as part of the total carbon present (Personal communication, Hallin, 2019), and the shape of the peak detection curves for total carbon analysis indicated an inorganic carbon contribution of $\leq$ ~30 % for NIC1 and NIC2 soils, and $\leq$ ~10 % for LLAN1 soils.

2.2.3. Drop shape and penetration imaging using goniometer measurements

Time-lapse images of the complete infiltration of a dispensed, detached water drop over time were obtained using a KRUSS Easydrop FM40 goniometer. A 1000 μl syringe was set up to dispense a drop of chosen volume (20, 50, 80 or 100 μl) at a rate of 200 μl min^{-1}. Images were collected every 3–6 s depending on the rate of penetration and water repellency of the soil being studied. Contact angles were obtained using Drop Shape Analysis (DSA) software and a polynomial method was selected as the most appropriate for measurements as it can adapt to a range of contour shapes at the three-phase contact.

The volume of water remaining on the soil as the drop penetrated was calculated as follows. Fifteen image frames were selected at equal time intervals chosen to cover the penetration process. These were converted into negative images in IrfanView (www.irfanview.com) and enlarged and printed to approximately A4 size on 1 mm graph paper for measurement, using the width of the goniometer syringe tip, measured using electronic callipers, as a 'scale bar' for calibration. The drop volume remaining was calculated by splitting the drop printed image into 2 mm high segments and the lengths for each were recorded to the nearest mm. The volume for each of these cylindrical segments was calculated and the volume of individual segments summed to give the drop volume. As soil grains cover the surface of the water drop, the drop will sit slightly lower than the initial soil surface in the small crater created from the movement of grains up and around the drop. Therefore, part of the drop volume is hidden from view and the volume obtained by the method above is slightly less than the true volume of water remaining on the soil. So a small correction, made by visually estimating the depth of the crater from the shape of that part of the drop which was visible and calculating the volume therein using the method above, was made to the data to correct for this hidden volume. This 'hidden volume' was never $>$ 15 % of the total drop volume and then only for NIC2 soil which is the least repellent and where water penetrates the soil rapidly; for the remaining soils the hidden volume was $<$ 10 %. The volume of the drop which had penetrated the soil was obtained by subtracting the volume remaining from the initial volume.

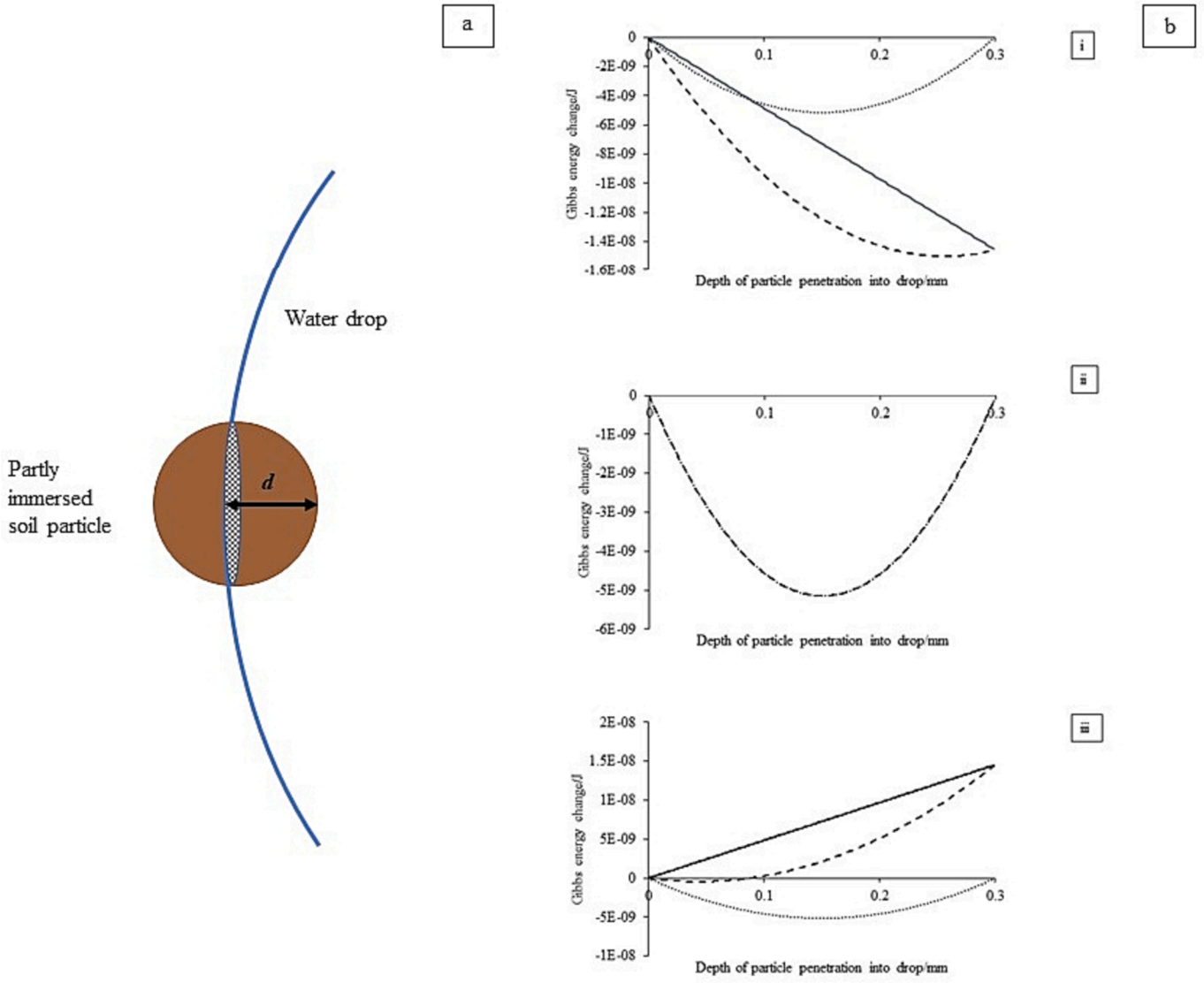

Fig. 2. Gibbs energy change for the loss of liquid–vapour interface and increase of solid–liquid interface as a soil grain penetrates into the surface of a water drop for a single spherical particle. **a)** Wetting of a spherical particle as it is taken into a water drop to depth *d*. **b)** Gibbs energy change (J) for a single soil particle of 0.15 mm radius penetrating into a 100 μl drop (mm) during the wetting process, and (i) where $\theta = 45°$, (ii) where $\theta = 90°$ and (iii) where $\theta = 135°$. The Gibbs energy change from the loss of liquid–vapour interface is given as a dotted line; the Gibbs energy change for the increase of solid–liquid interface is given as a solid line; and the overall Gibbs energy change (summation of previous two terms) is given as a dashed line. The particle will penetrate the water drop to the point where $(\partial G/\partial(\text{depth})) = 0$, i.e. the slope of the dashed line in the diagram is zero.

2.2.4. Time-lapse imaging of water drops penetrating soil

A Wessex WSA1 optical microscope fitted with a Brunel Microscopes Ltd Eyecam Plus camera eyepiece was used to take time-lapse images of water drops penetrating soil.

2.2.5. Water drop penetration time

The Water Drop Penetration Time (WDPT) test, as described by Letey (1969) and later in depth by Doerr (1998), with water repellency classifications based on those by Bisdom et al. (1993) was used to characterise the water repellency of the soils. A constant temperature and relative humidity room at 20–22 °C and relative humidity 40–52 % was used. Samples and solutions were left to equilibrate for a minimum of 24 h prior to testing (Doerr et al., 2002). Soil samples were placed in plastic Petri dishes and gently tapped to create a level surface, with enough soil to allow sufficient depth for full penetration of drop. Six drops of distilled water of a given volume were dispensed on to the soil surface at timed intervals. Drops were dispensed from a height < 5 mm to avoid soil displacement upon contact and the time from initial contact to full infiltration recorded.

2.2.6. Mass removal of soil grains over time – A 'start-stop' methodology

The aim of the experiment was to measure the mass of soil grains wetted at different intervals of penetration over time. Before experimentation samples were left to equilibrate for 48 h in a controlled climate room at 20–22 °C and relative humidity 40–52 %. Each soil sample was placed on an analytical balance and the balance tared. The weight of the soil sample prior to each drop being dispensed on to the surface was recorded, followed by the weight immediately after, 6 drops were dispensed for each sample interval. For each soil tested a series of intervals were sampled based on the overall WDPT for that soil. For example, a soil with a 5-minute WDPT was sampled every 30 s, whereas a soil with a 15-minute WDPT was sampled every 60 s. After the appropriate time had elapsed, a pre-weighed cotton bud was brought into contact with the water drop and the water and soil grains that had

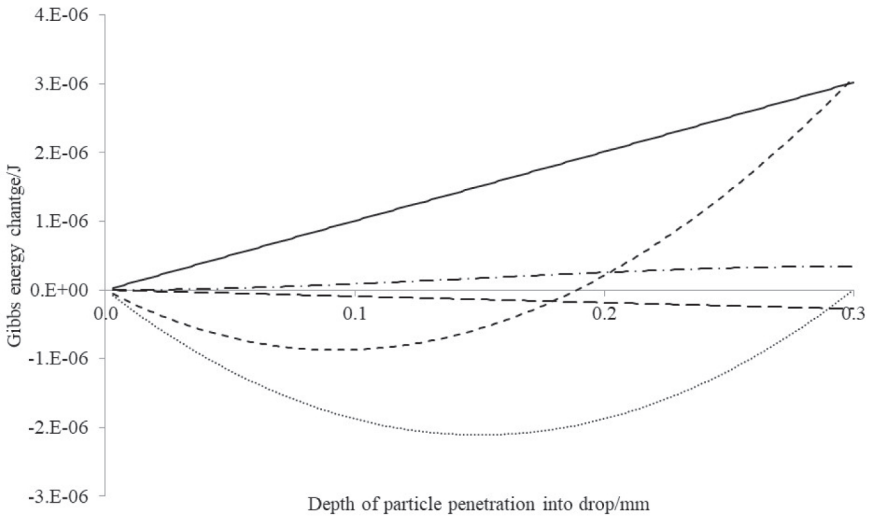

Fig. 3. Gibbs energy change (J) for a single sheet of close-packed particles, with depth of particle penetration into the drop (mm) during the wetting process, where θ = 111°, particle radius = 0.15 mm, drop volume = 100 μl; showing the gravity term as a long dash. The Gibbs energy gained from the loss of liquid–vapour interface is given as a dotted line; the Gibbs energy gained by the increase of solid–liquid interface is given as a solid line and the overall Gibbs energy (summation of terms) is given as a dashed line.

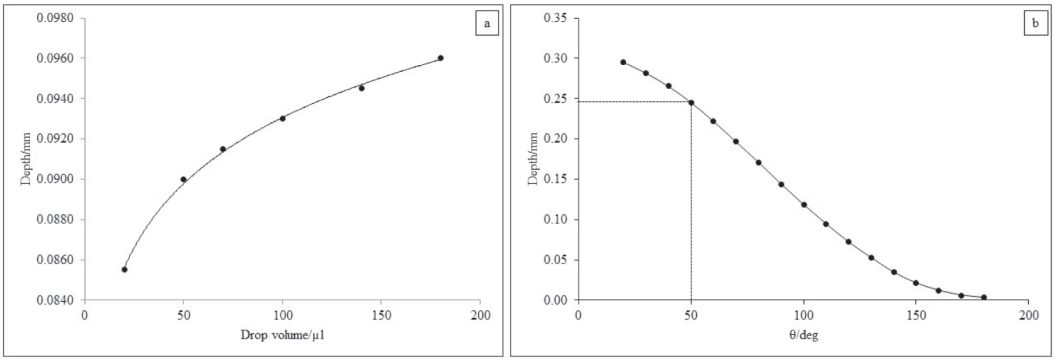

Fig. 4. Dependence of the depth of water drop penetration upon (a) drop volume and (b) contact angle for a water drop on close-packed spheres. **a)** Depth of the water drop on close-packed spheric particles of 0.15 mm radius against drop volume for θ = 111° (the contact angle for paraffin wax on a flat surface). **b)** Depth of water penetration against soil contact angle (θ) for 100 μl drop on 0.3 mm diameter particles (The dashed lined shows the 0.15 × 1.63*r* (0.245 mm) penetration depth, and corresponding theta of 50°).

been wetted adhered to the cotton bud and were removed for weighing (Fig. 1a).

The method was easily reproduced, and the cotton bud was effective at removing the water drop and attached wetted soil grains.

2.2.7. Sinter based water drop penetration time through different thickness of soil

In these experiments the soil was layered on top of a glass sinter disc (see Fig. 1b). This acted as a hydrophilic layer which presents a very low barrier to water penetration, and so the time measured for infiltration gives a good approximation of the time for the water drop to penetrate through the soil layer only. Different depths of soil, as determined by soil mass distributed over the measured surface area of the sinter, were placed in 18–20 mm diameter grade 3.0–4.0 (40–120 μm) glass sinter funnels and the time taken for water drops to infiltrate the soil recorded. A constant temperature and relative humidity room at 20–22 °C and relative humidity 40–52 % was used. The soil samples were weighed into small glass vials and placed in the constant temperature-humidity room for 48 h prior to testing. Drops of 20, 30, 50 and 80 μl were used with a minimum of 3 drops for each depth tested.

2.2.8. Loose- and settle-packed density

Loose- and settle-packed bulk density measurements were made as follows. An empty, stoppered, 10 ml glass volumetric flask was weighed. Soil was then added to the flask until the sample reached the 10 ml line. The flask was then stoppered and the weight recorded, and this weight was used to calculate the loose-packed density. Next the stopper was removed and flask gently tapped, causing the soil to settle and pack more tightly, additional soil was then added to the flask until it reached the 10 ml calibration line and no further tapping would create any extra space. The sample was then re-weighed and the settle-packed density calculated.

2.2.9. Profilometer

UKC (wettable) soil was sprinkled onto a square of adhesive tape attached to a glass microscope slide. The slide was tapped to remove any loose grains and the process repeated until a close packed covering of soil grains was achieved. Profilometer measurements of this soil surface were made using a Dektak profilometer with a 12.5 μm stylus and a manual moving platform. Profile data was collected over 10,000 μm lengths and at 25 μm spaced intervals.

2.2.10. Dimensions of wetted soil pellets

Dimensions of the soil pellets at different stages of water penetration, using liquid nitrogen to freeze the water drops at different times of penetration, were obtained using AUC (wettable) soil, with the height

and depth of the frozen pellet measured using electronic callipers. Soil samples were placed into small glass vials and tapped gently to give a level surface. A water drop was then dispensed onto the soil surface. At a set time the glass vial with sample was carefully lowered into liquid nitrogen and left there for approximately 60 s. The frozen pellet was turned out from the glass vial for measurement.

3. Theoretical considerations

3.1. First stage of soil water interactions: Adhesional wetting

3.1.1. Energy terms, total energy change, and depth of particle penetrating into the surface of a water drop for a single spherical particle

Consider the first stage of wetting in which a soil particle makes contact and is partially 'taken into' a water drop, i.e. the drop and particle adhere, Fig. 2. For simplicity, initially we ignore any gravitation energy terms and assume a spherical particle for which the difference in diameters between particle and drop is large enough that the drop can be considered flat across the diameter of the particle, and that the increase in liquid–vapour interface of the drop arising from the immersion of the particle in the drop is so small as to be negligible. (When the particle enters the drop the increase in effective volume of the drop, i.e. drop volume plus volume of particle inserted, increases the liquid–air interface; e.g. if a particle the same size as the drop was completely inserted then the volume enclosed by the liquid surface would be twice the original drop volume and the area of the liquid-vapour interface would increase commensurately).

The portion of the particle of radius r taken into the water drop to a penetration depth d (see Fig. 2a) is a spherical cap with area $2\pi rd$ (Wolfram Mathworld, 2019), and the change in energy in making the solid–liquid surface formed is given by Eq. (1) below:

$$\Delta G_{SL} = \left(\gamma^{SL} - \gamma^{SV}\right)2\pi rd \tag{1}$$

where: ΔG_{SL} is the change in Gibbs energy of the solid–liquid(water) interface, γ^{SL} is the surface tension of the solid–liquid(water) interface, γ^{SV} is the surface tension of the solid-vapour(air) interface, r is the radius of the particle and d is the depth of penetration of the soil particle into water.

The area of the circle across the interface plane of the spherical cap (Wolfram Mathworld, 2019) and resultant change in energy from the loss of liquid–vapour surface area is given by Eq. (2):

$$\Delta G_{LV} = \gamma^{LV}\left(2rd - d^2\right) \tag{2}$$

where: ΔG_{LV} is the change in Gibbs energy of the liquid(water)-vapour (air) interface, γ^{LV} is the surface tension of the liquid(water)-vapour (air) interface, r is the radius of the particle and d is the depth of penetration of the soil particle into water.

For this situation the Gibbs energy at any penetration depth, d, is given by the sum of two terms: the first term is associated with the increase in solid–liquid interface from the formation of the spherical cap and the second term is associated with the decrease in liquid–vapour interface which is equal to the area of the circle of the particle at the depth of contact. Fig. 2b shows both energy terms and their summation for a particle of 0.15 mm radius, and contact angles, (θ), of 45° (i), 90° (ii) and 135° (iii) respectively. The particle will move into the drop until $(\partial G/\partial(\text{depth})) = 0$, and so the depth to which the particle penetrates the drop is determined by the contact angle (θ). For a particle with $\theta = 90°$ taken into an infinitely large drop the particle penetrates up to the halfway point as this gives the greatest decrease in liquid–vapour surface area; for $0 < \theta < 90°$ the particle penetrates further but is never fully covered; for $\theta > 90°$ the particle penetrates to a shallower depth; while for $\theta = 180°$ it does not penetrate at all.

3.1.2. Energy terms, total energy change, and depth of drop penetrating into the surface for a hemisphere drop wetting a single layer of close-packed spheres

The Gibbs energy change involved in the wetting of a single layer of particles can be estimated for a hemisphere of water sitting on homogenous, close-packed, single sheet of spherical particles using the following approximations.

1) The drop is a hemisphere and retains this shape throughout the wetting process. The choice of a hemisphere for all soils is a convenience, it allows comparisons for equal area of water/soil contact for all soils. We recognise that strongly water repellent soils have a smaller initial contact area than less water repellent soils (see Fig. 5) (Balshaw, 2019), but the interfacial interactions, which are the major energetic factors involved, all vary linearly with contact area. Hence the shapes of the energy curves in Fig. 5 will remain essentially the same irrespective of contact area, only the absolute values of the energies involved i.e. the scale of the y axis in Fig. 5 will vary. No allowance is made for the increased surface area of the drop due to changes in the curvature of the surface upon contact with the soil.
2) The soil is made up of uniform, smooth, spherical particles with a packing density of close-packed spheres (Chang and Wang, 2010).
3) As the drop moves over the particles in this initial stage it does so with no lateral spread, and when accounting for gravitational energy (which is only a small contributor to the overall energy) the centre of mass of the hemisphere moves by the depth of penetration even though the particles will occupy some of the volume of the base of the hemisphere.
4) The increase in volume of the hemispherical drop as soil grains penetrate into the hemisphere causes an increase in the liquid–vapour surface area. This is a relatively small factor, and we estimate this from the surface area of a hemisphere composed of liquid plus volume of particles penetrating the liquid.

Fig. 3 gives diagrams for a representative example of particles with radius 0.15 mm and drop volume of 100 μl with a wax coating with contact angle of 111°, which corresponds to that for paraffin wax (Balshaw et al., 2021). Note that the relatively small energy contributions from gravity and the increasing total volume as particles penetrate the drop work in opposite directions, and thus effectively cancel one another out. Also, while gravity is not a major energy term it does have some influence on the depths to which water drops of different volumes will sit on the soil grains, with larger drops settling slightly deeper into the soil as shown in Fig. 4a.

While soil is not a collection of close-packed identical spherical particles, the general ideas of the competing energy terms considered here, general patterns of behaviour, and their dependence on surface contact angle, give a useful insight into the initial water soil interactions following contact between a water drop and real soil.

Kinetically, adhesional wetting to a surface of unchanging θ is very rapid. On the time scales of our experiments it is essentially instantaneous as soil and water make contact.

3.2. Second stage of soil water interaction: The transition from adhesion to infiltration

The next step in the process must involve the water drop penetrating through the first layer of soil particles adhering to it into the second and subsequent layers.

Previous research (Douglas et al., 2007; Diehl and Schaumann, 2007) has suggested for spreading wetting to occur in water repellent soils, the non-polar organics present on the surface of the soil grains will have to undergo chemical changes or reorientation of molecules to permit the penetration of the water wetting front into the soil profile. The rate (change in area wetted per unit time) for the wetting of a surface undergoing such a change will depend on two factors: 1) the rate constant

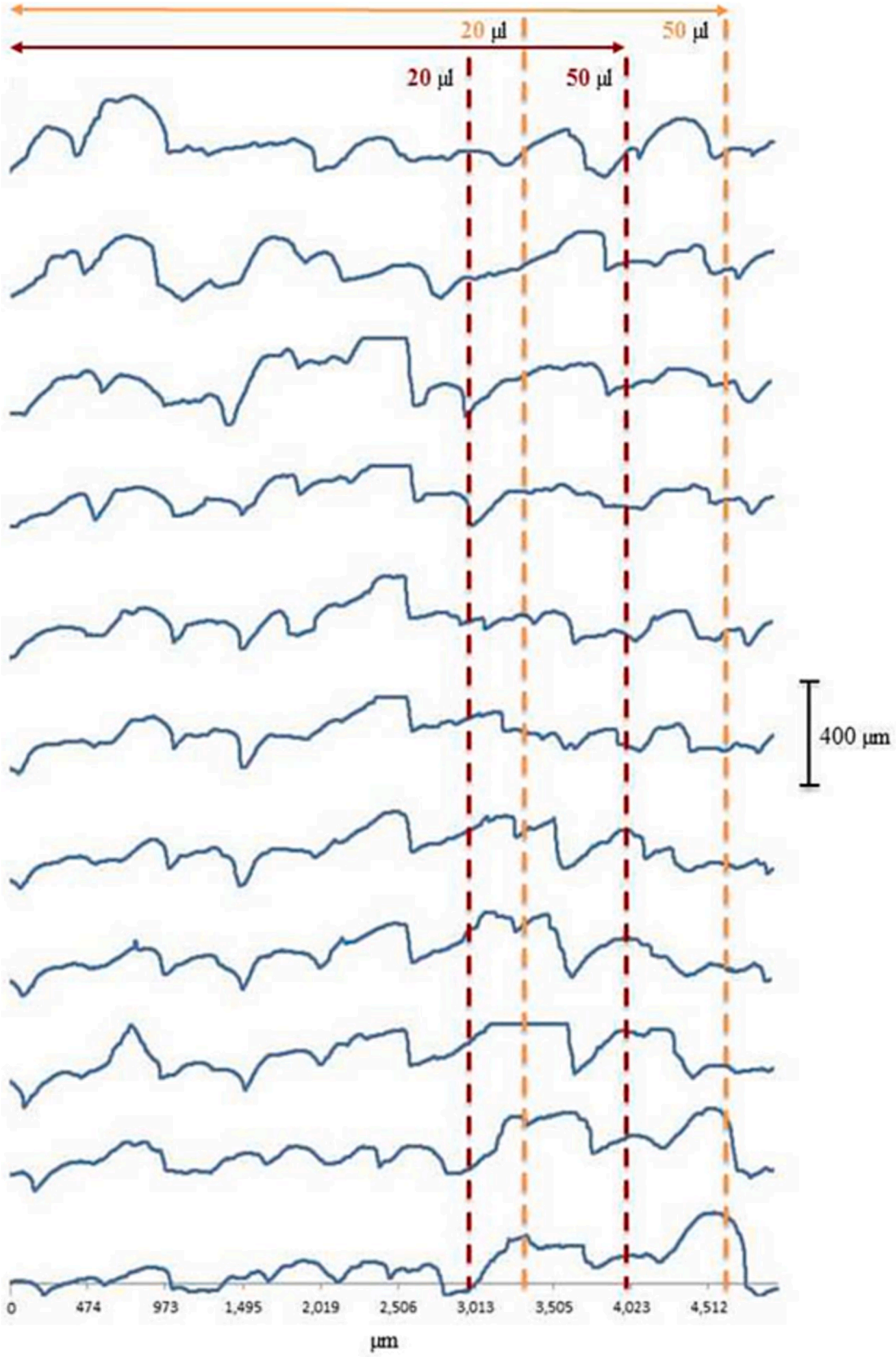

Fig. 5. Cross-sectional profiles from profilometer measurements on UKC soil showing surface roughness; 10 mm long scans at 25 µm spaced intervals, with 400 µm vertical scale marker shown. Approximate diameters of the contact circles for 20 and 50 µl drop on NIC2 (orange) which is a strongly repellent soil, and NL1 (red) which is a severely-extremely repellent soil, obtained from goniometer images, are also shown.

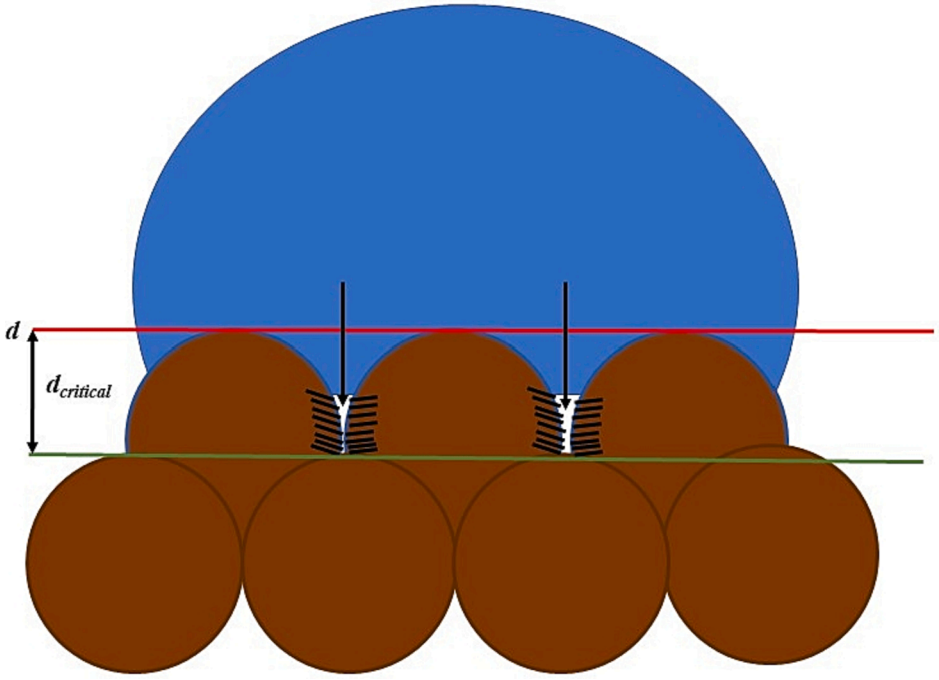

Fig. 6. Schematic of water drop sitting on soil grains. Branching interstitial wetting and penetration into bulk soil cannot occur until hatched area undergoes a change in hydrophobicity to permit water flow. The movement of water from the depth from where the water drop is initially sitting on the grains to the critical depth where it reaches the second layer of grains is controlled by this change in θ to $\theta_{critical}$.

for the rearrangement of the surface molecules, and 2) the length of the contact front between soil and water, i.e.

$$Rate = kL_{CF(t)} \tag{3}$$

where k is the rate constant for wetting, and $L_{CF(t)}$ is the length of the contact front at time t; and k is a rate constant of the usual form.

$$k = Ae^{(-Eact/RT)} \tag{4}$$

where A is the pre-exponential factor, E_{act} the activation energy, R, the Gas Constant, and T temperature in Kelvin. The relatively low activation energies measured for soil wetting indicate that the surface reorganisational processes involved are physical in nature rather than the breaking of chemical bonds (Diehl and Schaumann, 2007; Balshaw, 2019). Because of the way the drop sits on the soil, the initial contact length, $L_{CF(t)}$ when $t = 0$, will be smaller the more water repellent the soil, all other things being equal.

The transition from adhesional wetting to branching interstitial wetting occurs as the drop covers the soil particles from initial contact sufficient to reach a depth over the first contact layer to allow access to the surface of particles below this layer. Shirtcliffe et al. (2006) give this depth, for close-packed spheres of radius r, as $2(2/3)^{1/2}r$ (i.e. 1.63r) and, using a geometric approach to determine free energy changes, they calculate a contact angle of 50.73° to reach this depth. The depth of water penetration against contact angle for 100 μl drop using the energetic approach given here is shown in Fig. 4b, from which a critical contact angle to reach this depth of 0.245 mm is calculated to be 50° which is in good agreement with that calculated by Shirtcliffe et al. (2006).

Based on the calculation assumptions underlying Fig. 4b for spherical, homogenous, close-packed, spheres a critical contact angle of ≤ ~50° (identified as $\theta_{critical}$ in the following discussion) would be necessary for the water to make immediate contact with the second layer of spheres. However, soil is not made up of particles which are uniform in size and shape, nor are they necessarily close-packed. Some idea of the surface characteristic of natural soil, is given by the surface profile of a layer adhering to a strip of adhesive tape shown in Fig. 5.

In a loose- or settled-packed arrangement with a distribution of particle sizes there will be local variations in distances between first and second soil layers, leading to a distribution of such distances beneath a water drop. While the precise nature of this distribution will determine the overall rate of contact with the second layer of soil particles, the smaller of the distances will be the most critical, thus $\theta_{critical}$ for a natural soil is expected to be larger, perhaps significantly larger depending on particle size and shape distribution, than 50°. Whatever the actual value of $\theta_{critical}$, in a water repellent soil with $\theta > \theta_{critical,}$ a reduction of the initial contact angle to $\theta_{critical}$, thought to be associated with molecular restructuring, is required to allow water contact to move from the first contact layer into the second layer, and then into bulk soil, as illustrated schematically in Fig. 6.

3.3. Third stage of soil water interaction: Penetration into bulk soil

3.3.1. Theoretical considerations

A kinetic model for water moving through a uniform array of uniform spheres could be built around uniform sequential vertical movement through subsequent layers, with movement from each layer to the next inhibited by the same need to match a constant $\theta_{critical}$ (Shirtcliffe et al. 2006), however, for a natural soil, with a distribution of particle sizes, shapes, and probably surface hydrophobicities, the regularity of the array, and with it regularity of water movement, is lost within a relatively short distance. So, once water penetrates into bulk soil, filling of vacant soil interstices is not limited to vertical flow only, can occur from many directions, and is expected to lead to lateral spreading of wetting. Furthermore, since routes which are fastest i.e. those involving the largest local $\theta_{critical}$, will dominate the process, then the degree of molecular rearrangement required for interstitial wetting is probably less demanding than that required for wetting to extend from the first to second soil layers.

Since water moves in between soil particles and wets them in interstitial wetting there is no change in the liquid–vapour area, therefore, the overall Gibbs energy change for this process, ΔGs is given as

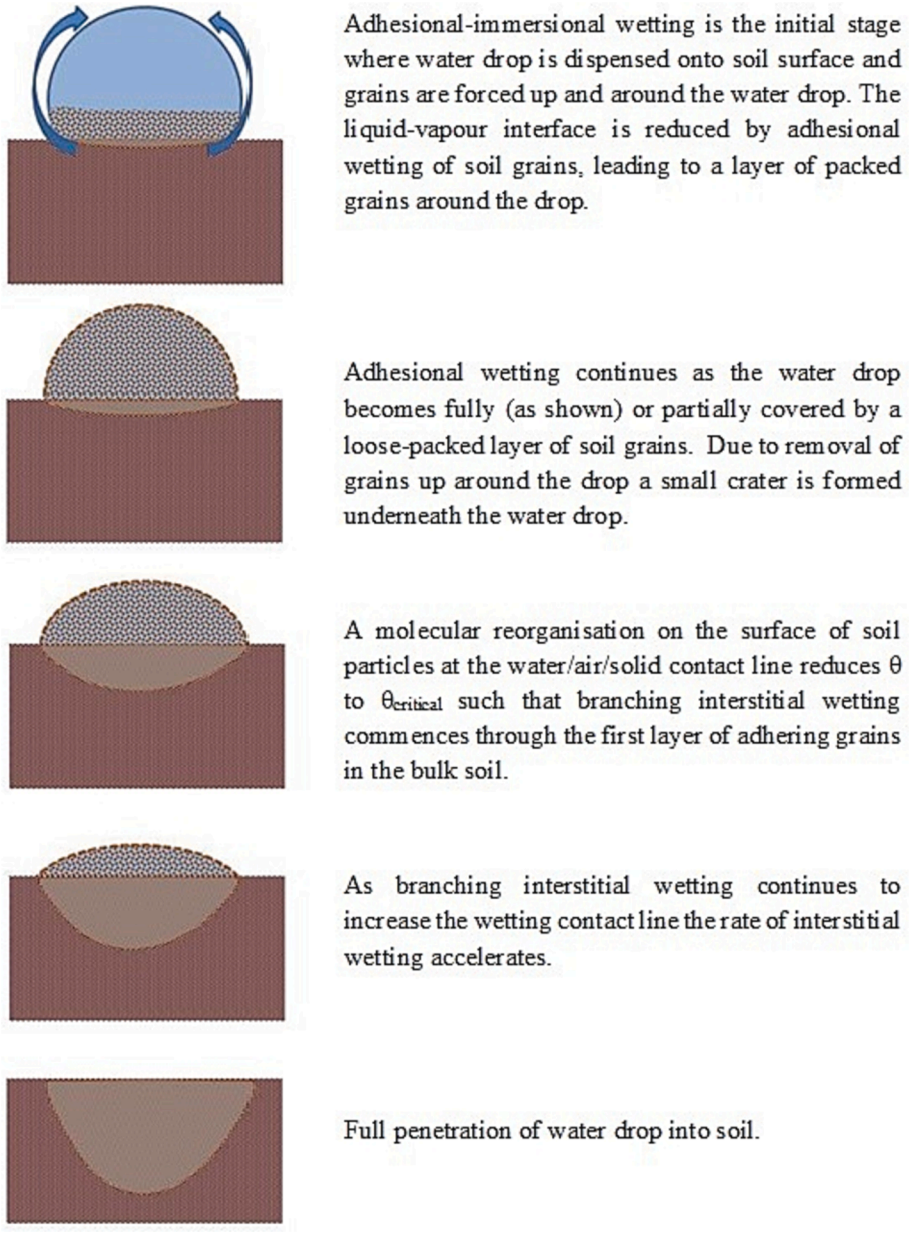

Fig. 7. Schematic showing the proposed wetting processes in a water repellent soil.

(Equation (5):

$$\Delta G_s = \Delta_{area}\left(\gamma^{SL} - \gamma^{SV}\right) \tag{5}$$

where: ΔGs is the change in Gibbs energy for interstitial wetting, Δ_{area} the change in area wetted, γ^{SL} is the surface tension at the solid–liquid (water) interface and γ^{SV} is the surface tension at the solid-vapour(air) interface.

From energetic considerations alone, interstitial wetting can occur for any contact angle where $\theta < 90°$ and will not occur for $\theta > 90°$ so, irrespective of $\theta_{critical}$, for cases where $\theta > 90°$, molecular rearrangement of surface molecules along the contact front is required before penetration can occur.

Consider the scenario where $\theta \leq \theta_{critical}$. Here rapid infiltration through the first layer of soil particles around the drop would be expected, followed by rapid branching interstitial wetting through the pores of the soil; water penetration would be seen as a single continuous process. However, if $\theta > \theta_{critical}$ rapid infiltration cannot occur, therefore the transition from adhesional wetting to interstitial wetting requires some change in the chemical nature of the solid–liquid interface i.e. molecular restructuring. We might then expect to be able to see the separate stages of water penetration experimentally: i.e. a rapid initial adhesional wetting, followed by an induction period while molecular reorganisation occurs before movement of water beyond the first layer of wetted particles into the second layer of particles can occur, and then the accelerating process of branching interstitial wetting, as the water drop penetrates into the soil. Fig. 7 gives a schematic summary of the proposed process.

4. Experimental results and discussion

4.1. Soil characterisation

Table 1 gives soil source locations and physical characteristics. To aid the reader, in subsequent discussion water repellency class is given in parentheses after the soil name where useful.

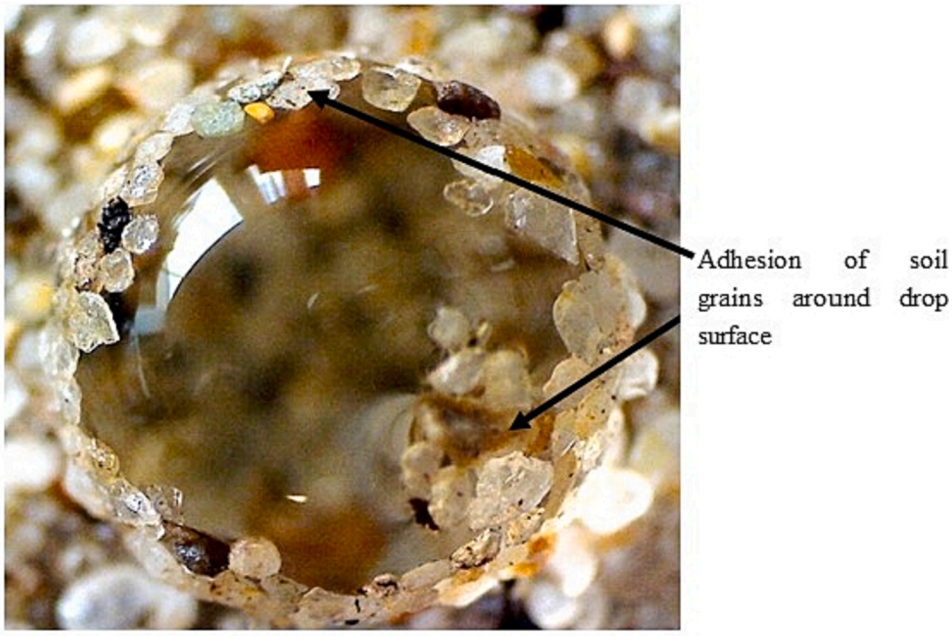

Fig. 8. Optical microscopy image of water drop (20 μl) on NIC1 soil showing the adhesional stage of the wetting process with grains adhered to the drop surface.

4.2. Optical microscopy and time-lapse images

Optical microscopy provides visual confirmation of the initial adhesional wetting stage in water repellent soils, as shown in Fig. 8 for NIC1 (severely) soil. where loosely packed soil particles can be seen adhered to, and partly taken in to, the water drop. Over time soil particles are observed jostling underneath the water drop, which results in them being forced up and around the drop. During this process it appears that the drop begins to penetrate into the soil, but, initially at least, this is due to the drop sitting lower than the initial soil surface in the small crater that has formed as soil particles are displaced upwards from underneath the drop. During the WDPT tests it was observed that this process occurred at different rates depending on the severity of the water repellency of the soil. For example, a layer of soil particles covered the drop on the lesser water repellent NIC2 (strongly) and LLAN1 (strongly) soils much more rapidly than for the high repellency NIC1 (severely) and NL1 (severely-extremely) soils. It is worth noting that for NL1 a full coverage of the drop with soil particles often did not occur before the drop began to infiltrate into the soil.

It is the forces of surface tension which drive the movement of soil particles from underneath the drop and allows them to jostle and move such that the drop is covered by as many accessible particles as is energetically and kinetically possible. As soil particles adhere to the drop surface it causes a loss in water-vapour interface which is replaced by the creation of a soil–water interface. Calculations of the energetics of this process indicate that the energy released through the destruction and formation of these interfaces is enough to lift soil particles (of the sizes found in soils used here) to the top of a 100 μl drop, although this does not include any consideration of inter-particulate or particle-water friction inhibiting movement.

We note an interesting asymmetry in the behaviour of soil particles adhering to the drop on the top of the drop and those beneath; those on the top do not end up being completely wetted and taken into the drop whereas those at the bottom do. Soil particles on top of the drop almost always remain in place adhering to the drop until they are deposited onto the soil surface when the drop penetrates completely into the soil. This is because to completely wet the particles on the top of the drop requires the reformation of the relatively high energy water-vapour interface over the particle, whereas for particles at the bottom what is formed is a new liquid–solid interface at the next layer of particles and there is no increase in water-vapour interface. So, the asymmetry is not so much between particles adhering to the top or bottom of the drop, but rather one between particles which have no adjacent contacting layers of particles and ones that do.

Table 2
Initial mass of soil wetted (within 8 s) per soil type and drop volume.

Drop volume (μl)	Mass wetted (g)			
	NIC2 (Strongly)	LLAN1 (Strongly)	NIC1 (Severely)	NL1 (Severely-extremely)
20	0.0175	0.0152	0.0155	0.0052
50	0.0516	0.0176	0.0242	0.0078
80	0.0450	0.0225	0.0276	0.0118
100	0.0729	0.0354	0.0374	0.0158

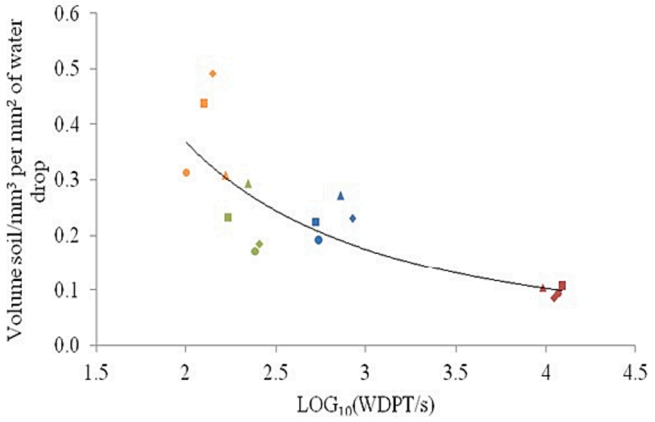

Fig. 9. Initial volume of soil (mm^3) per mm^2 of water drop against log water drop penetration time for NIC2 (strongly) (orange) and LLAN1 (strongly) (green) NIC1 (severely) (blue), and NL1 (severely–extremely) (red). Triangle (20 μl), diamond (50 μl), circle (80 μl) square (100 μl) soils at different drop volumes. The curve has been included just as a guide for the eye.

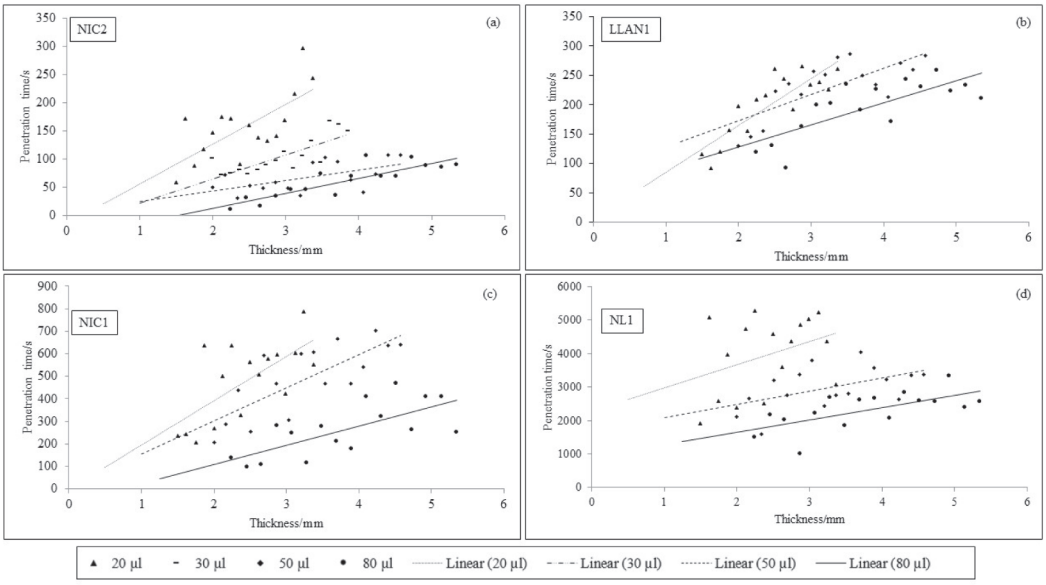

Fig. 10. Global plot of sinter water drop penetration time data, based on an average measurement from three drops per data point. **(a)** NIC2 **(b)** LLAN1 **(c)** NIC2 **(d)** NL1. Where, 20 µl is shown as triangles and corresponding linear fit is dotted, 30 µl is shown as dashes and corresponding linear fit is dash dot dot, 50 µl is shown as diamonds and corresponding linear fit is dash and 80 µl is shown as circles and corresponding linear fit is solid.

4.3. Initial mass pick up (mass removal experiments)

The masses of soil particles adhering to the drop after ~ 8 s contact, are given in Table 2.

Using these and soil packed-density data we can estimate the volume of soil adhering per unit surface area of the drop, and these values are plotted against $\log_{10}$(WDPT/s) in Fig. 9 (the choice of a log scale for WDPT is for convenience only, it has no theoretical significance).

The data show that for the least repellent soil (NIC2, strongly), there is a 3–4 times greater volume of soil taken up per unit surface area of the water drop, compared to the most repellent soil (NL1, severely-extremely). The data here reflects observations made during the WDPT tests whereby soil particles are picked up and cover a water drop more rapidly for a less repellent soil compared to a more repellent one. This can be explained by the polarity of the soil surface and the relevant surface energies involved (Jaycock and Parfitt, 1981; Rigby et al., 1986); a less repellent soil will have a more polar surface compared to a more repellent soil and therefore more energy is released in the exchange of interfaces as solid and liquid surfaces come into contact for a less repellent soil than a more repellent soil.

4.4. Water drop penetration time through layers of soil of different thicknesses

If the concept of a multistage process with a kinetic barrier to the transition from adhesional wetting to branching interstitial wetting is correct then, in its simplest form, a plot of time taken to penetrate against thickness of soil should result in a positive intercept corresponding to the time required for the kinetic barrier to be overcome, i.e. the data should show an induction period. Fig. 10 shows such plots for the four soils studied, obtained from drop penetration times through different thickness of soil on sinters.

The data are quite scattered, and a number of equations of varying complexity give comparable correlation coefficients, but a linear fit is simple, and, for this data, gives as good a fit as any other equation. We propose then a relationship between overall penetration time, t_{pen}, and thickness of soil, T_{soil}, of the form:

$$t_{pen} = t_{inf} + t_t T_{soil} \quad (6)$$

Table 3
Intercepts and slope – sinter data.

Soil	Drop volume/µl	Intercept (s)*	Slope (s mm^{-1})*
NIC2	20	−17 ± 35	72 ± 14
	50	2 ± 15	19 ± 4
	80	−34 ± 13	25 ± 3
LLAN1	20	38 ± 28	62 ± 11
	50	99 ± 36	42 ± 11
	80	14 ± 27	45 ± 7
NIC1	20	−25 ± 110	210 ± 42
	50	−12 ± 89	151 ± 27
	80	−111 ± 65	94 ± 17
NL1	20	2442 ± 667	610 ± 256
	50	1679 ± 442	397 ± 134
	80	656 ± 295	421 ± 79

* Error estimate is one standard deviation.

where t_{inf} is the time between first contact and branching interstitial wetting to start i.e. the induction period, and t_t is the time taken to penetrate a fixed thickness of soil by branching interstitial wetting.

The most obvious observation to be drawn from Fig. 10 is that overall penetration times for all soil thicknesses increase as drop volume decreases, but resolving this to show the dependence upon t_{inf} and t_t, i.e. intercept and slope in Fig. 10, is difficult because of the scatter in the data. Only for the most repellent soil, NL1 (severely-extremely), do the data show a clear positive intercept (which increases as drop volume decreases). For the rest, intercepts are scattered around zero, and the high experimental errors in intercept determination prevent any definite conclusions to be drawn for these soils. We note however, an experimental complication to consider, in that the movement of soil grains from underneath the drop also causes the drop to move through the soil layer, although this is by displacement not penetration, and the effect of this is to reduce the thickness of the soil layer the drop must penetrate to contact the sinter. We have made no correction for this for the data shown in Fig. 10, but if such a correction could be reliably applied the effect would be to reduce the x- axis value of each point on any given plot by the same fixed amount. This would lead to an increase in the intercept for each plot but leave the slope unchanged, and this means that all intercepts in Table 3 are systematically low to some extent.

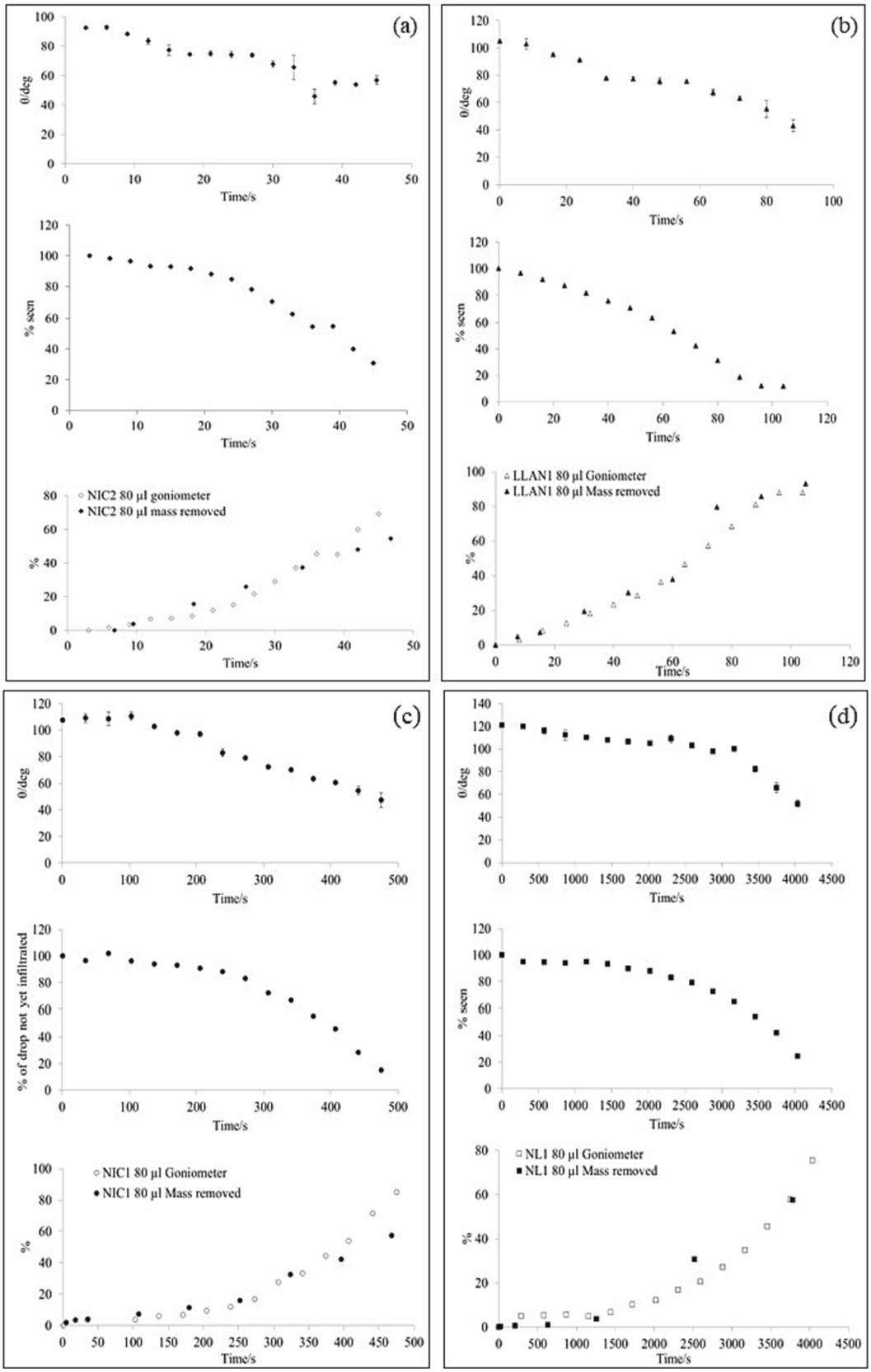

Fig. 11. Contact angle, fraction of water drop penetrated, and mass of soil wetted as a function of time for (a) NIC2, (b) LLAN1, (c) NIC1, (d) NL1. 80 µl drops. In each instance: (Top) Contact angle (θ) from time-lapse goniometer images against time. (Middle) Fraction of drop not yet infiltrated over time. (Bottom) Fraction of total mass removed against time, along with fraction of drop infiltrated against time, i.e. inverse of Middle plot, for comparison (data for mass removed adjusted to allow for same WDPT timescales, see text).

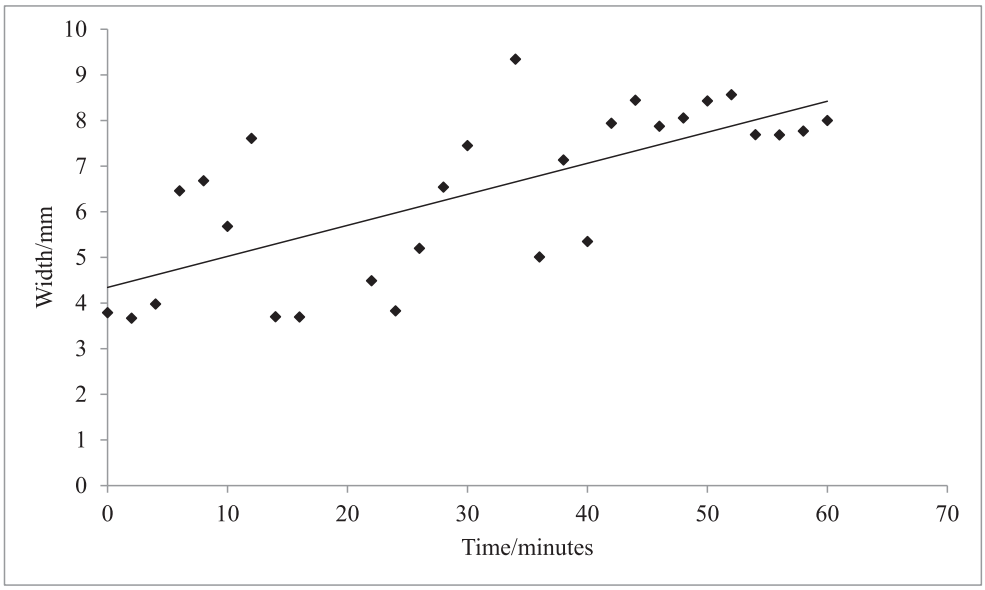

Fig. 12. Width of wetted soil pellet against penetration time, obtained using AUC (wettable) soil by measurement of frozen pellet obtained at specified time by immersion in liquid nitrogen. After full penetration the depth of the pellet was ca. 7 mm.

Interpreting the variation in time to penetrate a fixed thickness of soil, t_t, (which is the inverse of rate of penetration), is also difficult because of the scatter in the data, but we note that for all soils t_t for 20 μl drops is greater than that for larger drop volumes.

However, for the highly repellent soil, NL1 (severely-extremely), the data does show experimental resolution of the stages in the wetting of the soil. For NL1 both the intercept, i.e. induction period, and slope, i.e. time for interstitial wetting through a given thickness of soil, increase as drop volume decreases.

From the data on different drop volumes, we suggest the gravitation energy term may play some part in determining the rate of interstitial wetting for all soils studied. And we suggest the gravitation energy term may also influence the rate of transition from adhesional to interstitial wetting, at least for the most repellent soil studied.

4.5. Time-dependent measurements of contact angle, volume of water penetrated, mass of soil wetted, and size of water/wetted-soil pellet

Fig. 11 shows contact angle, fraction of water drop penetrated, and mass of soil wetted as a function of time for all soils studied. (Note the data set for mass removal is not directly comparable to that from the goniometer because the tests were carried out under different conditions; the mass removal experiments were conducted in a constant temperature/relative humidity room whereas the goniometer was restricted to the laboratory conditions where it was set up. Therefore, to make a meaningful comparison between data, the data has been adjusted by normalising the time axis for mass removal to give the same WDPT values as the goniometer experiments.).

In previous work we have shown that the measured contact angle for soils using a goniometer designed for flat surfaces is not the true contact angle for the soil–liquid interface but rather a composite made up of the true contact angle plus an additional term arising from how the water drop sits on the soil surface (Balshaw et al., 2021). Even so, the variation in contact angle over time gives some measure of the progress of the wetting process. Time-lapse images taken using a goniometer, can also be used to provide a measurement of the volume of the water drop which has not yet penetrated the soil over time.

The data is consistent with the model proposed in that all measurements show a process that begins slowly but accelerates with time. For the water repellent soils NIC1 (severely) and NL1 (severely-extremely) in particular, there is a significant initial period of time during which there is little change in any of the measured properties, a period of time we interpret as corresponding to the transition from adhesional wetting to interstitial wetting as the most significant kinetic barrier to the overall process, i.e. the transition from θ to $\theta_{critical}$, is overcome.

The rate of penetration is further increased by lateral spread of water in the soil, as shown in Fig. 12. A comparison of the bulk water soil contact area before and after penetration for a 100 μl drop on AUC (wettable) soil used to obtain the data in Fig. 12, gives an initial contact circle area of $\pi(2.2)^2 = 15$ mm^2, and a final contact area, assuming a spherical cap of 4 mm radius and height of 7 mm (after full penetration the depth of the pellet was 7 mm), of $\pi(4^2 + 7^2) = 204$ mm^2; i.e. a fourteen fold increase in bulk contact area, contact line, and hence rate of water penetration, at the end of the process compared to that at the start. This is consistent with the observation of an accelerating rate of penetration once the drop has broken through from the first contact layer into bulk soil.

5. Conclusions and implications

From theoretical considerations of the energetics and kinetics of the processes by which a water drop makes contact and then penetrates into soil, a three-stage model has been proposed, advancing the understanding of how water eventually infiltrates water repellent soils. It involves the following: 1) Adhesional wetting as soil and water first make contact, which is essentially instantaneous on the time scale of our experiments. 2) A kinetic barrier transitional stage in which molecular reorganisation of organics on soil reduces the contact angle from θ to $\theta_{critical}$ which allows water to contact soil particles in layers below those initially in contact. The time for this to occur depends on θ and the rate of any molecular reorganisation required to reduce θ to $\theta_{critical}$, with the latter dependent upon particle size distribution and packing. 3) Branching interstitial wetting as water infiltrates into the bulk soil. The time for this to occur depends on θ, and the rate of any molecular reorganisation required to reduce θ to 90°.

Studies of optical microscopy, mass of soil initially wetted, penetration time through layers of soil of different thicknesses, time-dependent measurements of contact angle, volume of water penetrated, and mass of soil wetted, all give results consistent with this model. However, only for highly water repellent soils can distinct stages in wetting be clearly resolved experimentally, presumably because only these soils have a high enough kinetic barrier in the transitional stage for

good separation between stages. For less water repellent soils, while the general time dependent behaviour remains consistent with the model, the distinction between the three stages is not so easy to resolve.

The findings presented here have relevance to the amelioration of soil water repellency. Any additive which increases packing density by increasing particle size heterogeneity would be expected to lead to a reduction in $\theta_{critical}$ and it is suggested the mechanism by which the addition of clay or other fine particulates lowers soil water repellency (e.g. Cann, 2000) may involve a reduction in $\theta_{critical}$, as fine particulates sit in between soil grains and reduce the depth to which a water drop must sit on the soil before contacting underlying layers of soil particles.

CRediT authorship contribution statement

Helen M. Balshaw: Conceptualization, Methodology, Formal analysis, Investigation, Writing - original draft, Writing - review & editing. **Peter Douglas:** Conceptualization, Formal analysis, Methodology, Writing - original draft, Writing - review & editing. **Stefan H. Doerr:** Conceptualization, Writing - original draft, Writing - review & editing.

Declaration of Competing Interest

The authors declare that they have no known competing financial interests or personal relationships that could have appeared to influence the work reported in this paper.

Data availability

Data will be made available on request.

Acknowledgement

Helen M. Balshaw thanks the Engineering and Physical Sciences Research Council (EPSRC) Doctoral Training Academy (DTA) grant for funding (EP/L504865/1).

References

Balshaw, H.M., 2019. New approaches to the study of hydrophobicity and wetting of soils: methods and theories. Swansea University, Swansea. PhD Thesis.
Balshaw, H.M., Douglas, P., Doerr, S.H., 2021. On the cause and correction of the anomalously high contact angles measured on soils and granular materials. Geoderma 391, 114973.
Bisdom, E.B.A., Dekker, L.W., Schoute, J.F.T., 1993. Water repellency of sieve fractions from sandy soils and relationships with organic material and soil structure. Geoderma 56, 105–118.
Bond, R.D., 1972. Germination and yield of barley when grown in a water-repellent sand. Agron. J. 64, 402–403.
Cann, M.A., 2000. Clay spreading on water repellent sands in the south east of South Australia – promoting sustainable agriculture. J. Hydrol. 231–232, 333–341.
Chang, H. and Wang, L. 2010. A Simple Proof of Thue's Theorem on Circle Packing. https://arxiv.org/abs/1009.4322v1 - accessed February 2019.
Dekker, L.W., Ritsema, C.J., 1994. How water moves in a water repellent sandy soil. 1. Potential and actual water repellency. Water Resour. Res. 30 (9), 2507–2517.
Dekker, L.W., Ritsema, C.J., 1996. Variation in water content and wetting patterns in Dutch water repellent peaty clay and clayey peat soils. Catena 28, 89–105.
Dekker, L.W., Ritsema, C.J., Oostindie, K., 2000. Extent and significance of water repellency in dunes along the Dutch coast. J. Hydrol. 231–232, 112–125.
Diehl, D., Schaumann, G.E., 2007. The nature of wetting on urban soil samples: wetting kinetics and evaporation assessed from sessile drop shape. Hydrol. Process. 21, 2255–2265.
Doerr, S.H., 1998. On Standardizing the 'water drop penetration time' and the 'molarity of an ethanol droplet' techniques to classify soil hydrophobicity: a case study using medium textured soil. Earth Surf. Proc. Land. 23, 663–668.
Doerr, S.H., Shakesby, R.A., Walsh, R.P.D., 1998. Spatial variability of soil hydrophobicity in fire-prone eucalyptus and pine forests, Portugal. Soil Science. 163, 313–324.
Doerr, S.H., Shakesby, R.A., Walsh, R.P.D., 2000. Soil water repellency: its causes, characteristics and hydro-geomorphological significance. Earth Sci. Rev. 51, 33–65.
Doerr, S.H., Dekker, L.W., Ritsema, C.J., Shakesby, R.A., Bryant, R., 2002. Water repellency of soils: the influence of ambient relative humidity. Soil Sci. Soc. Am. J. 66, 401–405.
Doerr, S.H., Llewellyn, C.T., Douglas, P., Morley, C.P., Mainwaring, K.A., Haskins, C., Johnsey, L., Ritsema, C.J., Stagnitti, F., Allinson, G., 2005. Extraction of compounds associated with water repellency in sandy soils of different origin. Aust. J. Soil Res. 43 (3), 225–237.
Douglas, P., Mainwaring, K.A., Morley, C.P., Doerr, S.H., 2007. The kinetics and energetics of transitions between water repellent and wettable soil conditions: a linear free energy analysis of the relationship between WDPT and MED/CST. Hydrol. Process. 21 (17), 2248–2254.
Franco, C.M.M., Clarke, P.J., Tate, M.E., Oades, J.M., 2000. Hydrophobic properties and chemical characterisation of natural water repellent materials in Australian sands. J. Hydrol. 231–232, 47–58.
Hallett, P.D., Douglas, J.T., Ritz, K., Wheatley, R.E., Young, I.M., 2001. Plant root and microbial derived soil water repellency. In: Macfarlane-Smith, W.H., Heilbronn, T. (Eds.), In: Scottish Crop Research Institute Annual Report 2000/2001, pp. 148–151.
Jaycock, J., Parfitt, G., 1981. Chemistry of interfaces. Ellis Horwood series in chemical science, Chichester, England.
Jex, G.W., Bleakley, B.H., Hubbell, D.H., Munro, L.L., 1985. High humidity induced increase in water repellency in some sandy soils. Soil Sci. Soc. Am. J. 49 (5), 1177–1182.
Letey, J., Carrillo, M.L.K., Pang, X.P., 2000. Approaches to characterize the degree of water repellency. J. Hydrol. 231–232, 61–65.
Letey, J. 1969. Measurement of contact angle, water drop penetration time, and critical surface tension. In: DeBano, L.F., Letey, J. (Eds.), Proceedings of a Symposium on Water Repellent Soils, May 6-10. 1968, Riverside, CA, pp. 43-47, 354p.
Wolfram Mathworld, 2019. http://mathworld.wolfram.com/SphericalCap.html - accessed February 2019.
McGhie, D.A., Posner, A.M., 1981. The effect of plant top material on the water repellence of fired sands and water-repellent soils. Aust. J. Agr. Res. 32, 609–620.
McIntosh, J.C. and Horne, D.J. 1994. Causes of repellency: I. The nature of the hydrophobic compounds found in a New Zealand development sequence of yellow brown sands. In: Proceedings of the 2nd National Water Repellency Workshop, August 1994, Perth, Western Australia, pp. 8-12.
Rigby, M., Smith, E.B., Wakeham, W.A., Maitland, G.C., 1986. The Forces Between Molecules. Clarendon Press, Oxford.
Ritsema, C.J., Dekker, L.W., 1996. Water repellency and its role in forming preferred flow paths in soils. Aust. J. Soil Res. 34, 475–487.
Roberts, F.J., Carbon, B.A., 1972. Water repellence in sandy soils of southwestern Australia. 2. Some chemical characteristics of the hydrophobic skins. Aust. J. Soil Res. 10, 35–42.
Shirtcliffe, N,J., McHale, G., Newton, M.I., Pyatt, F.B. and Doerr, S.H. 2006. Critical conditions for the wetting of soils, Applied Physical Letters. 89 art. 09410.